Check for updates

Study on adsorption of phosphate from aqueous solution by zirconium modified coal gasification coarse slag†

Baoguo Yang,[ab] Fenglan Han,*[c] Zuoming Xie,[a] Zhe Yang,[a] Fengcheng Jiang,[d] Sen Yang[a] and Yilian Li (ID) *[a]

Zr-modified materials have an adsorption affinity for phosphate ions, but because of the cost of carrier materials, they are difficult to apply on a large scale. Herein, coal gasification coarse slag (CGCS) was used as a carrier material and modified with Zr, and its dephosphorization performance was studied. A series of adsorbents with different CGCS/$ZrOCl_2 \cdot 8H_2O$ mass ratios were prepared, from which the adsorbent with a CGCS/$ZrOCl_2 \cdot 8H_2O$ mass ratio of 5 : 4 (denoted as CGCS-Zr4) was identified as the most promising for phosphate adsorption. The specific surface area of CGCS-Zr4 was much greater than that of raw CGCS (100.12 *vs.* 12.43 m^2 g^{-1}). CGCS-Zr4 showed good adsorption selectivity towards phosphate when competitive anions co-existed, and exhibited good reusability; the adsorption capacity in the fourth adsorption–desorption cycle remained above 11.98 mg g^{-1}. The adsorbent was also suitable for the continuous treatment of up to 830 and 743 bed volumes of synthesised and actual wastewater, respectively. The results of Fourier-transform infrared and X-ray photoelectron spectroscopy indicated that CGCS not only plays the role of a carrier, but also that Ca and Al in CGCS play an important role in phosphate adsorption. Compared with other carrier materials such as biochar and synthetic zeolite, CGCS has the advantages of a large stockpile, low cost, and easy availability. In addition, the preparation of CGCS-Zr4 is simpler and more energy-saving. Zr-modified CGCS is a promising dephosphorization material.

1. Introduction

Phosphates from industrial emissions, agricultural runoff and household activities lead to excessive phosphate in natural water bodies, resulting in eutrophication.[1] Various methods have been applied to remediate phosphate pollution, including precipitation,[2] adsorption,[3] ion exchange,[4] and biological processes.[5] Adsorption is the most popular of these technologies owing to its economy, efficiency, and reliability.[6,7] In the adsorption method, the choice of adsorbent is crucial. In recent years, Zr-modified materials have received increasing interest for phosphate removal, because Zr has a high affinity for phosphate ions,[8] and Zr-modified materials have strong acid

resistance and good stability.[9] However, most Zr-based adsorption materials are sourced from biochar,[10] activated carbon,[8] synthetic zeolite,[11] natural minerals,[12] and other carriers.[13,14] In terms of modification research, Zr-modified materials have very high raw material and production costs, and the preparation processes are complicated, requiring high temperatures, large amounts of chemical reagents. Therefore, there is a pressing need to find cheap and easily available carrier materials for the production of adsorbents with simpler, more environmentally friendly, and more energy-efficient preparation processes. A good candidate for the carrier material is coal gasification slag (CGS), a general solid waste formed as a by-product of the coal gasification process, with large stockpiles. Notably, CGS contains large amounts of Ca, Al, and Fe, which provide effective adsorption sites for adsorbates.

With increasing demand for coal-based chemicals and gaseous fuel production, coal gasification technology is becoming increasingly important.[15,16] However, large amounts of CGS are produced as a byproduct.[17] CGS contains both coarse and fine slag (denoted as CGCS and CGFS, respectively), which have different chemical compositions.[18] There are about 700 different types of coal gasifiers in production.[19] Coal consumption has exceeded 95 million tons and the annual formation of CGS in China exceeds 33 million tons.[20] The

[a]Hubei Key Laboratory of Yangtze River Basin Environmental Aquatic Science, School of Environmental Studies, China University of Geosciences, NO. 68 Jincheng Street, East Lake High-Tech Development Zone, Wuhan, 430078, P. R. China. E-mail: yl.li@cug.edu.cn

[b]Ningxia Geophysical and Geochemical Survey Institute, Yinchuan 750001, China

[c]School of Materials Science and Engineering, North Minzu University, Yinchuan 750021, China. E-mail: 625477897@qq.com

[d]Institute of Resource and Environment, Henan Polytechnic University, Jiaozuo, Henan 454003, China

† Electronic supplementary information (ESI) available. See https://doi.org/10.1039/d2ra02263j

accumulation of this solid waste poses a threat to the environment. Thus, the effective use of CGS has become a critical and complex issue for governments and scholars.

In recent years, an increasing number of studies have been conducted on the use of CGS to prepare adsorption materials. For example, an adsorbent comprising mesoporous glass microspheres has been produced from CGFS, which successfully adsorbed methylene blue.[21] CGFS has also been used to prepare deodorant for the removal of volatile organic compounds.[22] CGS has been used to prepare carbon-silica mesoporous composites by hydrochloric acid leaching, and their application in nitrate removal was investigated.[17] An amine-modified CGFS adsorbent has been fabricated and used to capture CO_2 gas.[23] To date, the use of CGS to synthesise adsorption materials has mostly been focused on the development of carbon–silicon mesoporous materials, extraction of unburned carbon, and preparation of zeolites. However, the preparation of these materials requires many chemicals, such as acids and bases, or a high roasting temperature, which can create new waste and are not environmentally friendly.

To date, most research on CGS has focused on CGFS, with relatively few studies on CGCS; in particular, there have been no reports on the adsorption behaviour of CGCS for phosphates in waste water. Herein, a novel Zr-modified CGCS composite for phosphate adsorption was synthesised using CGCS by a facile, energy-saving and environmentally-friendly method, which does not require extensive use of chemicals, such as, acids and bases, or high-temperature roasting. Applying CGCS to phosphate removal will not only benefit the treatment of phosphate pollution in water bodies, but also realise the reuse of solid waste resources. Providing new candidates for the utilisation of CGCS is of great significance to the resource utilisation of CGS. In this study, we focus on: (1) the synthesis of novel composite and the characterisation of the related materials; (2) systematic evaluation of the performance of Zr-modified CGCS for phosphate adsorption from aqueous solutions under different adsorption conditions, such as phosphate concentration, pH, and co-existing anions; and (3) the role of Ca, Al, and Fe in CGCS in the process of dephosphorisation and revelation of the possible phosphate adsorption mechanism on Zr-modified CGCS.

2. Materials and methods

2.1. CGCS and chemicals

CGCS was collected from Shenhua Ningxia Coal Industry Group Co., Ltd, Ningxia, China. The raw material was ground for 20 min using a vibrating mill, followed by screening through a 200-mesh sieve and collection for subsequent experiments. The major components of CGCS are SiO_2 (55.5%), Al_2O_3 (15.6%), CaO (10.9%), Fe_2O_3 (8.1%), MgO (2.26%), C (2.9%), Na_2O (1.52%), K_2O (1.23%), TiO_2 (0.72%), others (1.27%).

Chemicals, such as hexaammonium heptamolybdate tetrahydrate, potassium dihydrogen phosphate, potassium tartrate semihydrate and zirconium oxychloride were purchased from Tianjin Kemiou, China. All reagents were of AR-grade, and all solutions were prepared using deionized (DI) water and the pH

values were adjusted using 0.1 mol L^{-1} $H^{-1}Cl$/NaOH. Anhydrous KH_2PO_4 was used to prepare a phosphate stock solution.

2.2. Preparation of Zr-modified CGCS

To improve the activity of Al, Ca, Fe and other substances in CGCS while introducing hydrated zirconia, an *in situ* and one-step synthesis method was used, wherein NaOH was used as an alkali activator and precipitant. Before the synthesis, CGCS was washed with DI water to remove impurities and dried at 110 °C. The pre-treated CGCS (5 g) was mixed with the desired amount of $ZrOCl_2 \cdot 8H_2O$ in a 250 mL conical flask, 50 mL of DI water was added, and the mixture was blended using a magnetic stirrer for 1 h. Then, NaOH (1 mol L^{-1}) was added dropwise to the suspension until a pH of 10 was reached, and the mixture was continuously stirred for another 14 h. Following the centrifugation, the solid was washed with DI water, dried at 105 °C, ground, and preserved in a desiccator for further batch experiments.

Adsorbents with different mass ratios of CGCS to $ZrOCl_2 \cdot 8H_2O$ (5 : 0, 5 : 1, 5 : 2, 5 : 3, 5 : 4, 5 : 5, and hydrated zirconium oxide), were synthesised by the above methods, and are denoted as CGCS, CGCS-Zr1, CGCS-Zr2, CGCS-Zr3, CGCS-Zr4, CGCS-Zr5, HZO, respectively.

2.3. Adsorption experiments

2.3.1. Effect of CGCS/Zr mass ratio. To determine the influence of the CGCS/Zr mass ratio, 50 mg of each adsorbent was added to a (separate) 250 mL conical flask containing 50 mL of 35 mg L^{-1} phosphate. The initial pH of the solution was adjusted to 6.00 ± 0.03 by adding 0.1 mol L^{-1} HCl/NaOH. The vessels were shaken in a water-bath oscillator at 160 rpm for 24 h. After adsorption, the mixture was filtered through a 0.45 μm membrane syringe to analyse the residual phosphate concentration.

2.3.2. Batch experiments. The batch adsorption experiments (other than those to evaluate the pH effects, isotherms and kinetics) were conducted by adding 50 mg of CGCS-Zr4 to 50 mL of a 20 mg L^{-1} phosphate solution, which was then placed in a water bath oscillator with an agitation speed of 160 rpm for 24 h at 25 °C and pH 6 ± 0.03.

To evaluate the influence of wastewater pH on phosphate adsorption, adsorption experiments were conducted using a 40 mg L^{-1} phosphate solution, and the pH was adjusted in the range of 2–10 by adding 0.1 mol L^{-1} HCl/NaOH. The ionic strength of the solutions was studied by increasing the $NaNO_3$ concentration from 1 to 10 mM. The influence of co-existing anions and humic acid on the phosphate removal behaviour was assessed by adding $NaNO_3$, NaCl, $NaHCO_3$, and Na_2SO_4 solutions at concentrations of 1 and 10 mM, and humic acid concentrations at 20 and 40 mg L^{-1}. Adsorption isotherms were acquired within the initial concentration range of 5–50 mg L^{-1} at temperatures of 25 and 50 °C. Kinetic experiments were carried out to estimate the reaction time at adsorption equilibrium. In these experiments, 50 mg of adsorbent was added to 50 mL of 10 mg L^{-1} phosphate solution, and samples were

taken from the suspension at certain intervals for analysis of the residual phosphate concentration.

To examine the reusability of the CGCS-Zr4 adsorbent, four adsorption–desorption cycles were conducted as follow. In the adsorption step, 0.05 g of adsorbent was placed in a weighed, dry 250 mL conical flask, to which 50 mL of a 20 mg L^{-1} phosphate solution was added. The vessel was then, placed in a constant temperature (25 °C) water bath oscillator with an agitation speed of 160 rpm for 24 h. After the reaction, the concentration of the phosphate concentration remaining was measured, after which the adsorbent was washed with DI water until a neutral pH of supernatant was reached. The vessel was then dried and re-weighed and the mass of the adsorbent was calculated. In the desorption step, 50 mL of a 1 M NaOH solution was used as the eluent. The recovered adsorbent was then used in the next adsorption cycle.

2.3.3. Real wastewater adsorption test. Experiments were also conducted using actual phosphate-contaminated wastewater samples in a fixed-bed column. Water from a ditch near a residential area in Yinchaun (Ningxia Hui Autonomous Region, China) was sampled in November 2021. Column adsorption tests were carried out using a 30 mL syringe with an inner diameter of 1.5 cm. Glass wool was packed at the top and bottom of the syringe, between which 2 g of CGCS-Zr4 was filled with a bed height of 1 cm. To better observe the phosphate removal capacity of the adsorbent under continuous flow conditions, the phosphorus concentration of the ditch water was adjusted to 2 mg L^{-1}, and the influent was passed through the adsorbent at a flow rate of 2 mL min^{-1} under gravity. The treated wastewater was collected at certain time intervals in a 10 mL centrifugal tube, and the residual phosphorus concentration was determined.

2.4. Characterisation

The chemical composition of the CGCS was analysed using an X-ray reflective fluorescence (XRF) spectrometer (Panalytical Axios, Netherlands). The morphology and surface elements of the samples were characterised using scanning electron microscopy (SEM, Zeiss Sigma 500, Germany). X-ray diffraction (XRD, LabX XRD-6000, Japan) was conducted to analyse the crystal characteristics of the samples in a scanning range of 10°–80° at a scan speed of 2°/min. Fourier-transform infrared (FTIR) spectra were measured using a Thermo Scientific Nicolet iS5 in the range of 400–4000 cm^{-1}. A 3H-2000 PM 1 specific surface & pore size analyzer was used to examine the specific surface area and pore characteristics. The surface elemental composition was measured by X-ray photoelectron spectroscopy (XPS, Esca Lab 250Xi, USA) with a pass energy of 100.0 eV (Al $K\alpha$). The point of zero charge (pH$_{PZC}$) of the adsorbents was determined using the method described by Huang *et al.* (2020).[24]

The phosphate concentration was determined using molybdenum-antimony anti-spectrophotometric method on a PERSEE TU-1901 dual-beam ultraviolet visible spectrophotometer with a detection wavelength of 710 nm. The removal efficiency R (%) and adsorption capacity Q_t, were computed according to the equations given in Text S1 (ESI)†.

3. Results and discussion

3.1. Effects of CGCS/Zr mass ratio

To identify the optimal CGCS/Zr mass ratio, adsorbents with different mass ratios were synthesised. Fig. 1 indicates that the adsorption capacity increased with a decrease in the CGCS/Zr mass ratio; however, the rate at which the adsorption capacity increased gradually decreased, indicating a decrease in the contribution of Zr per unit mass to the adsorption capacity. Therefore, considering the contribution rate of Zr and the adsorption capacity of the obtained material, CGCS-Zr4 was selected for subsequent experiments. Compared with CGCS-Zr2, CGCS-Zr3, CGCS-Zr4, and CGCS-Zr5, pure hydrated zirconium oxide (HZO; ZrO(OH)$_2$) had a low adsorption capacity. The high adsorption capacity of Zr modified CGCS may benefit from the following: (1) the synergistic effect of Zr and CGCS, which was confirmed by FTIR and XPS analyses; and (2) the avoidance of ZrO(OH)$_2$ particle agglomeration, as the particles were well dispersed on the CGCS surface. Unmodified CGCS had a low adsorption capacity, whereas after Zr modification, the obtained adsorbent had a high adsorption capacity. Therefore, it can be concluded that the Zr-modification can significantly increase the adsorption capacity of phosphate.

3.2. Influence of pH and ionic strength

Fig. 2(a) displays the influence of pH on the phosphate adsorption behaviour of CGCS-Zr4. CGCS-Zr4 had good acid resistance and a high adsorption capacity (14.08–23.78 mg g^{-1}) within a broad pH range (pH 2–7). The adsorption of phosphate is evidently related to the solution pH, with the phosphate adsorption capacity increasing as pH decreased. Similar results have been reported for other adsorbents by other researchers.[8,25] Depending on the solution pH, the main forms of phosphate
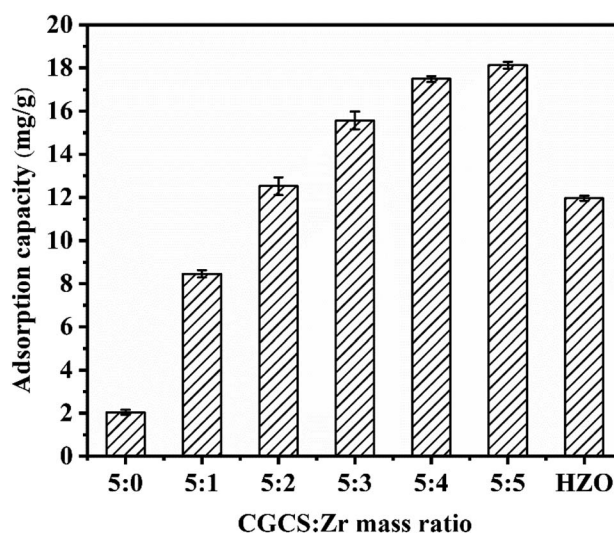

Fig. 1 Influence of CGCS/Zr mass ratio on phosphate adsorption in 35 mg L^{-1} phosphate solution (50 mL). Adsorption conditions: sorbent dose, 1 g L; temperature, 25 °C; pH = 6.0 ± 0.03; agitation speed, 160 rpm.
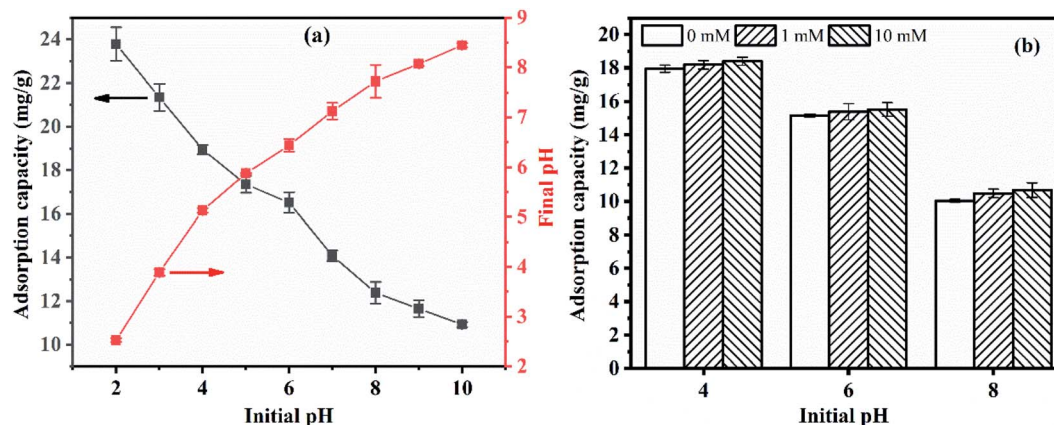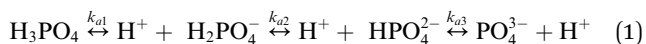
Fig. 2 Influence of (a) solution pH and (b)ionic strength-on phosphate adsorption performance by CGCS-Zr4. Adsorption conditions: adsorbent dose, 1 g L; reaction time, 24 h; temperature, 25 °C; agitation speed, 160 rpm; initial phosphate concentration, 40 mg L^{-1}.

are H_3PO_4, $H_2PO_4^-$, HPO_4^{2-}, or PO_4^{3-}, which is illustrated as follows:

$$H_3PO_4 \overset{k_{a1}}{\leftrightarrow} H^+ + H_2PO_4^- \overset{k_{a2}}{\leftrightarrow} H^+ + HPO_4^{2-} \overset{k_{a3}}{\leftrightarrow} PO_4^{3-} + H^+ \quad (1)$$

where the dissociation constants pK_{a1}, pK_{a2}, and pK_{a3} are 2.15, 7.20 and 12.33, respectively. According to the ionisation constant, negatively charged $H_2PO_4^-$ and HPO_4^{2-} are the dominant species at pH 2–10. The pH_{PZC} of CGCS-Zr4 is 8.41, as shown in Fig. S5.† These results indicate that the CGCS-Zr4 surface is positive when the solution pH is below pH_{PZC}, and negative when the solution pH is above pH_{PZC}. Given the high pH_{PZC}, the adsorbent has a positive charge in acidic, neutral, and weakly alkaline environments, which facilitates the adsorption of negatively charged phosphate anions ($H_2PO_4^-$ and HPO_4^{2-}). The electrostatic attraction between the negatively charged phosphate ions and positively charged CGCS-Zr4 surface promotes the adsorption of phosphates in the pH range of 2–8. However, with increasing pH, the number of binding sites with positive charges on CGCS-Zr4 decreases; thus, the electrostatic repulsion gradually increases, which hinders the adsorption of phosphates. Meanwhile, at high pH, OH^- ions compete with the negatively charged phosphates for binding sites, which reduces the phosphate removal efficiency.

The final pH increased in the range of 2–7 for CGCS-Zr4 (Fig. 2(a)), which is mainly attributed to ligand exchange between the phosphate ions and OH^- groups on the CGCS-Zr4 surface, as verified by FTIR spectroscopy. Through this ligand exchange, OH^- groups are replaced by phosphate ions, and the phosphates ions bind to the CGCS-Zr4 surface. Simultaneously, OH^- groups are released into the solution, resulting in an increased amount of OH^- in the solution. In comparison, in alkaline media (pH 8–10), OH^- tend to be adsorbed onto the surface of the adsorbent, and positively charged protons are released from the surface of CGCS-Zr4, thus decreasing the final pH.

The ionic strength may have different influences on the adsorption capacity in different pH environments. Therefore, solution pH values of 4 (representing a more acidic environment), 6 (the approximate pH of the mixture of water, CGCS-Zr4 and phosphate ions), and 8 (representing an alkaline environment) were selected to investigate the influence of ionic strength on the adsorption capacity of CGCS-Zr4 in different pH environments. As shown in Fig. 2(b), the adsorption capacity was either not affected or increased slightly as the ionic strength. If outer-sphere surface complexes formed, the adsorption capacity of phosphate would decrease as the ionic strength increases, whereas if inner-sphere complexes formed, the adsorption capacity would either stabilise or increase.[26] Thus, phosphate was adsorbed by CGCS-Zr4 to form inner-sphere surface complexes. This finding agrees with the mechanism inferred from the pH_{PZC} shift of CGCS-Zr4 after adsorption.

3.3. Effect of co-existing anions and humic acid

Natural waters or wastewater contain humic acid and various co-existing ions, including nitrate, bicarbonate, sulfate, and chloride.[27,28] Considering that natural water or wastewater will be used in practical applications, the influence of humic acid and coexisting anions on the phosphate adsorption behaviour needs to be considered. Thus, it is essential to investigate the selectivity of CGCS-Zr4 for phosphate anions, the effects of which are illustrated in Fig. 3.

The presence of various anions in the phosphate solution had no negative effect on the adsorption behaviour of CGCS-Zr4 towards phosphate, even at very high anion concentrations (concentration of 10 mM, *i.e.*, 15.5 times higher than that of phosphorus). Interestingly, the presence of anions actually promoted the adsorption capacity. Outer-sphere association caused by electrostatic interactions are strongly sensitive to anion concentration, whereas inner-sphere complexes tend to be insensitive to the concentration of coexisting anions.[29] Hence, the mechanism by which CGCS-Zr4 adsorbs phosphate is probably through the formation of inner-sphere surface complexes; a similar phenomenon has been reported previously.[30]

Humic acids are forms of natural organic matter and possess plenty of function groups; thus, they often affect the adsorption
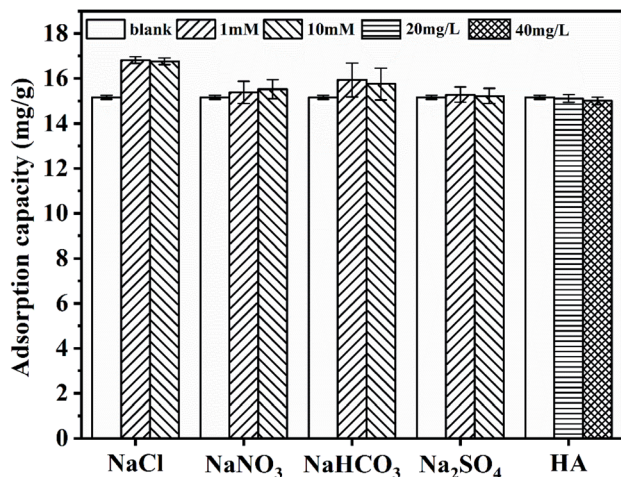
Fig. 3 Effect of coexisting anions and humic acid. Adsorption conditions: adsorbent dose,1 g L; reaction time, 24 h; temperature, 25 °C; agitation speed, 160 rpm; initial phosphate concentration, 20 mg L^{-1}.

properties of adsorbents. The phosphate adsorption behaviour of CGCS-Zr4 was not significantly affected by the presence of humic acid in the present study, and the negative effect was negligible in the present study. This may be ascribed to the inner-sphere complex adsorption mechanism of phosphate ions onto CGCS-Zr4 and the macromolecular structure of humic acid. As shown in Fig. 6, the average pore size of CGCS-Zr4 is 2.67 nm; therefore, it may be difficult for bulky humic acid molecules to enter the pores of CGCS-Zr4 to compete with phosphate anions for adsorption sites. Thus, even when high concentrations of humic acid and anions co-exist with phosphate, CGCS-Zr4 can still adsorb phosphate effectively. This suggesting it is a promising phosphate adsorbent for future practical utilisation.

3.4. Adsorption isotherms

Adsorption isotherms were obtained to illustrate the phosphate adsorption capacity of CGCS-Zr4 at different equilibrium concentrations. The adsorption capacity increased with increasing equilibrium concentration, as shown in Fig. S1,† and eventually tended to stabilise. Moreover, the adsorption capacity increased slightly at higher temperatures, demonstrating the endothermic nature of phosphate adsorption on the adsorbent surface.[25] In order to understand the adsorption mechanism between the adsorbent and adsorbate, equilibrium isotherm data were fitted by Langmuir and Freundlich isotherm equations, which are presented in Text S2 (ESI)†.

The Langmuir and Freundlich fitting results are given in Fig. S1,† and the fitting data of the two models and their corresponding parameter coefficients are listed in Table S1.† Both the Langmuir and Freundlich models can describe the phosphate adsorption isotherms on CGCS-Zr4, indicating that the adsorption of phosphate by CGCS-Zr4 may involve both monolayer and multilayer adsorption.[8,24] The values of $K_L > 0$ and $0 < 1/n < 1$ indicate that adsorption occurs easily, as displayed in Table S1†.[31] The maximum adsorption capacities (q_m)

of phosphate on CGCS-Zr4 were 19.81 and 22.37 mg g^{-1} at 25 and 50 °C, respectively. Compared with other Zr-modified materials, metal materials, and solid waste adsorbents studied by other researchers, as exhibited in Table S2,† CGCS-Zr4 has considerable adsorption capacity for phosphates.

3.5. Adsorption kinetics

To evaluate the effect of time on the CGCS-Zr4 adsorption behaviour, an adsorption kinetics experiment was conducted. Fig. S2† depicts the influence of adsorption time. Rapid adsorption occurred at the initial stage ($t \leq 3$ hours). The adsorption rate then tended to decrease (5 h later) until plateauing after 22 h. This phenomenon can be explained by two factors: the concentration of adsorbate and the number of adsorption sites of the adsorbent. In the initial stage, there were many vacant sites on the CGCS-Zr4 surface and a higher concentration gradient in the aqueous solution, which leds to a higher adsorption driving force at the solid–liquid interface.[24] As adsorption progresssd, the concentration of phosphate ions in the aqueous solution decreased continuously, which gradually diminished the diffusion force produced by the concentration gradient. Meanwhile, because the active sites on the adsorbent became occupied by phosphate ions, the number of available binding sites decreased, resulting in a decrease in the adsorption rate.

To explore the adsorption mechanism, various kinetic models were applied to explicate the experimental data. The equations of the three common models were presented in Text S3. The plots and parameters are given in Fig. S2 and Table S3,† respectively. By comparing, the R^2 values, the pseudo-second-order and Elovich equations were found to be more suitable than the pseudo-first-order equation for deciphering the adsorption mechanism, indicating that chemical adsorption occurred. The $q_{e,cal}$ value (8.233) was closer to the experimental data($q_{e,exp} = 9.14$), suggesting that the rate-determining step was governed by ion exchange or chemical adsorption, rather than mass transfer.[32] To further investigate the rate-controlling step and diffusion mechanism, intra-particle diffusion was considered. As shown in Fig. S2(d),† the line did not pass through the origin of the coordinates, and there were three adsorption phases, displaying a multi-linearity relationship. This indicates that adsorption occurs by a multi-stage adsorption process, and does not have a single intraparticle diffusion-determining step. The first phase with the largest slope, represents the boundary layer diffusion of phosphate anions from the solution to the CGCS-Zr4 surface. The second phase, which has a more gradual slope, corresponds to the intra-particle diffusion of phosphate from the solid surface to the binding sites. The third phase corresponds to the final equilibrium stage. From Table S3,† k_{id1} is greater than k_{id2}, meaning that external mass transfer or boundary layer diffusion is the primary rate-controlling step of the overall adsorption process, and intra-particle diffusion is a secondary rate-controlling step.[33]

3.6. Reusability performance

To explore the reusability of CGCS-Zr4, four rounds of adsorption–desorption experiments were performed. The adsorption

capacity decreased slightly with increasing number of cycles, as shown in Fig. 4. The decrease in adsorption capacity suggests phosphate ions may have bound strongly to some adsorption sites, making it difficult for these phosphate ions to be eluted in the desorption step using 1 M NaOH. As the number of cycles increased, the cumulative number of non-renewable sites increased, and the effective number of active sites of CGCS-Zr4 decreased accordingly, resulting in a continuous decline in the adsorption capacity. Nevertheless, only a relatively small proportion of the adsorption capacity was lost after four cycles. The adsorption capacity in the fourth cycle remained above 11.98 mg g^{-1}, indicating that CGCS-Zr4 has good reusability and is a promising adsorbent.
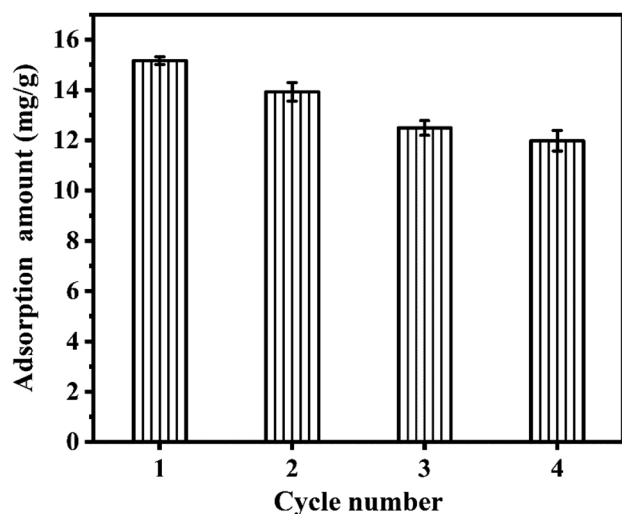

Fig. 4 Adsorption performance of CGCS-Zr4 over four adsorption cycles. Adsorption conditions: CGCS-Zr4 dose, 1 g L; initial phosphate concentration, 20 mg L; eluant, 50 mL of 1 M NaOH; reaction time, 24 h; temperature, 25 °C.

3.7. Real wastewater dephosphorisation test

To verify the practical usability of CGCS-Zr4, a column test was conducted to investigate its ability to treat synthesised and actual wastewater under continuous flow conditions, and the results are shown in Fig. 5. The main chemical components and pH of the actual wastewater (ditch water) before and after adsorption are listed in Table S4.† The content of TOC and the main cations in the ditch water (Ca^{2+}, K^+, Mg^{2+}, Na^+) decreased in varying degrees after adsorption. Notably, the phosphate ions were completely removed, and the content of fluoride ions decreased to a certain extent. However, there were no obvious changes in the content of other anions (Cl^-, NO_3^-, SO_4^{2-}). This indicates that the adsorbent can also remove TOC, metal cations (Ca^{2+}, K^+, Mg^{2+}, and Na^+) and fluorine ions from this system.

China's urban sewage control standard (GB 18918-2002) has a phosphorus concentration limit of 0.5 mg g^{-1}. Therefore, this was selected as the breakthrough point. Under the condition of a flow rate of 2 mL min^{-1}, empty bed volume of 3.462 mL, empty bed contact time of 1.73 min, 2 g of CGCS-Zr4 can continuously treat synthesised and actual wastewater over 830 and 743 bed volumes (BV), respectively. The amount of actual water treated by CGCS-Zr4 was less than that of simulated wastewater. This may be due to the reaction between CGCS-Zr4 and TOC, metal ions (Ca^{2+}, K^+, Mg^{2+}, Na^+) and fluorine ions in the actual water body, resulting in the relative reduction of phosphorus treatment capacity. In summary, CGCS-Zr4 can effectively treat actual low-phosphorous wastewater under continuous flow conditions.

3.8. Characterization

3.8.1. SEM-EDS. The SEM images of CGCS, Zr modified Coal Gasification Coarse Slag (CGCS-Zr4) and P-loaded CGCS-Zr4 are displayed in Fig. S-3. CGCS has an irregular block morphology with a smooth surface. In contrast, as presented in Fig. S3(b),† the shape of the irregular blocks changed upon Zr
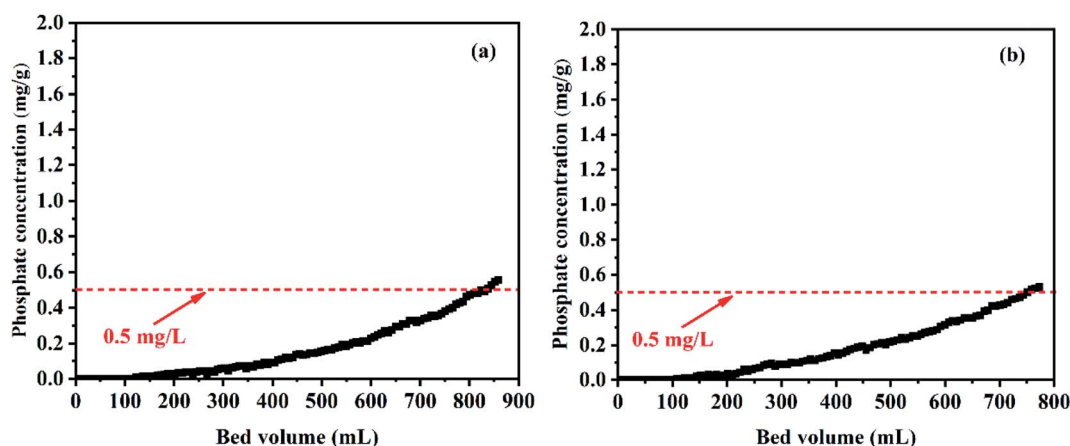

Fig. 5 Column breakthrough curve of phosphate from (a) synthesised wastewater and (b) ditch water onto CGCS-Zr4. Adsorption conditions: influent concentration, 2 mg L; flow rate, 2 mL min^{-1}, EBCT, 1.73 min; temperature, 25 °C.
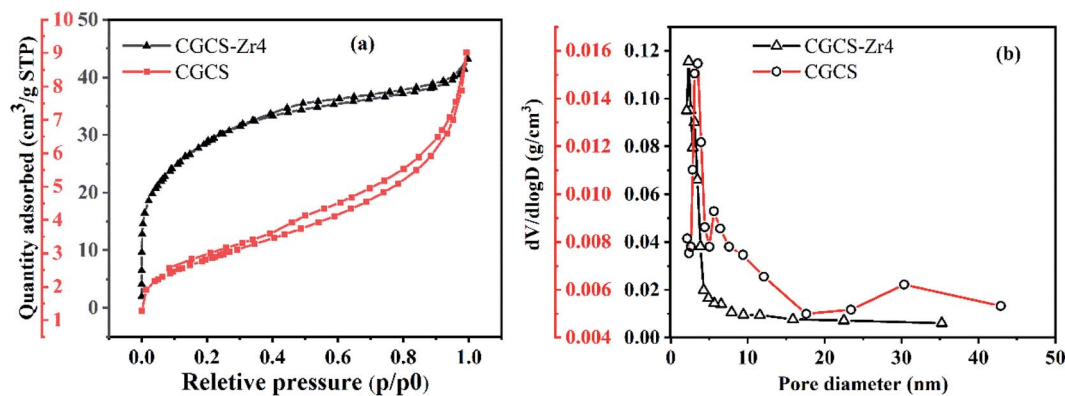
Fig. 6 (a) N_2 adsorption–desorption isotherms of CGCS and CGCS-Zr4; (b) pore size distribution curves of CGCS and CGCS-Zr4.

modification, and the surface of CGCS-Zr4 was rough, with many pits and holes. These morphological changes are beneficial for improving the phosphate adsorption capacity. These morphological changes may have been caused by the reaction between NaOH and aluminosilicates in CGCS during the preparation process. After the adsorption of phosphate ions (Fig. S3(c)),† the surface morphology did not change significantly.

Energy dispersive X-ray spectroscopy (EDS) results of the various materials are shown in Fig. S3.† The presence of Zr in the spectrum of Zr-modified CGCS proved that Zr successfully entered the CGCS substrate. In addition, comparing the elemental compositions of CGCS and CGCS-Zr4, the mass fraction of Si decreased significantly upon Zr modification, whereas the mass fraction of Zr increased. This result can be explained by the destruction of the crystal structure of silica during the synthesis process, with partial replacement of the silicon atoms were replaced by Zr. These results were confirmed by XRD and FTIR results. The presence of a P peak in the EDS spectrum after adsorption indicates the successful adsorption of phosphate ions onto the composite.

3.8.2. XRD. XRD images are shown in Fig. S4.† A wide diffraction dispersion was observed, which demonstrates that these materials were amorphous.[21] According to the variation in intensity of quartz peak for CGCS and CGCS-Zr4, it can be concluded that the crystal structure of quartz in CGCS was disrupted during Zr modification. Under alkaline conditions, the quartz structure was corroded and destroyed, allowing Zr to successfully enter the CGCS substrate. This is in accordance with the EDS results. The XRD pattern of CGCS-Zr4 did not change significantly after phosphate adsorption.

3.8.3. N₂ adsorption–desorption isotherms and BET-BJH analysis. As shown in Fig. 6(a), both raw CGCS and CGCS-Zr4 show type IV isotherms in terms of the IUPAC, indicating the presence of mesopores in the adsorption material. The hysteresis loops of raw CGCS and CGCS-Zr4 are of type H3 and H4, respectively.[34] This indicates that the pores could be slit-like pores.[1] The pores in raw CGCS might be formed by the accumulation of plate-like particles, whereas CGCS-Zr4 may produce slit pores similar to those generated by layered structures during the modification process. As illustrated in Fig. 6(b), the

Barrett–Joyner–Halenda (BJH) pore sizes of raw CGCS and CGCS-Zr4 are distributed in the mesoporous range, which agrees well with the N_2 adsorption–desorption isotherms. The average mesopore sizes of CGCS-Zr4 and CGCS are 2.67 nm and 5.7 nm, respectively. Nevertheless, the number of mesopores in CGCS-Zr4 was far greater than that in raw CGCS. The Brunauer–Emmett–Teller (BET) specific surface area of CGCS-Zr4 was 100.12 m^2 g^{-1}, which is much greater than that of raw CGCS (12.43 m^2 g^{-1}). The larger the specific surface area, the better the adsorption performance, because a larger specific surface area provides more binding sites. Thus, this further validates the better adsorption capacity of CGCS-Zr4 compared to that of CGCS.

3.9. Phosphate adsorption mechanism

3.9.1. FTIR. The infrared spectrum spectra of CGCS, CGCS-Zr and CGCS-Zr after phosphate adsorption are given in Fig. 7. In CGCS, the absorption bands located at 793 and 466 cm^{-1} are assignable to the stretching and bending vibrations of O–Si–O, respectively. The peak at 1055 cm^{-1} is attributed to Si–O–Al
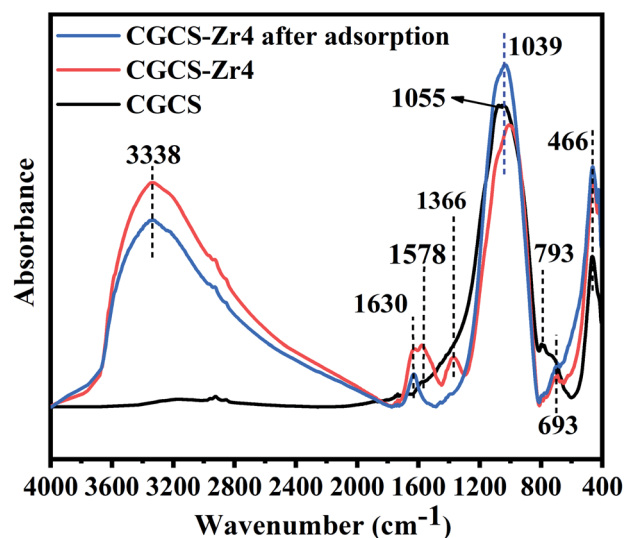

Fig. 7 FTIR spectra of samples.

asymmetric stretching vibration.[17] After Zr modification, additional peaks appeared at 3338 and 1630 cm^{-1}, which may represent the stretching and bending vibrations of –OH groups in CGCS-Zr4.[35–37] This may be attributed to the fact that the addition of sodium hydroxide destroys the original aluminosilicate structure, resulting in the formation of more metal oxide surface hydroxyl groups (M–OH) in CGCS-Zr4 (e.g., Al–O, Ca–O). The intensities of the peaks at 3338 and 1630 cm^{-1} were significantly weakened after the adsorption of phosphate ions on CGCS-Zr4, indicating that M–OH was involved in the

adsorption of phosphate. After Zr modification, the peak at 793 cm^{-1} for CGCS disappeared, and a new peak was detected at 693 cm^{-1}, indicating the partial corrosion of SiO$_2$ by NaOH and formation of ZrO(OH)$_2$ during Zr modification.[38] This is consistent with the XRD observations. After phosphate adsorption, the adsorption peaks corresponding to Zr–OH vibrations at 1578 and 1366 cm^{-1} vanished, indicating that ligand exchange occurred between the metal oxide surface (M–OH) and phosphates (H$_2$PO$_4^-$ and HPO$_4^{2-}$). Meanwhile, the intensity of the peak at 1039 cm^{-1}, which corresponds to the
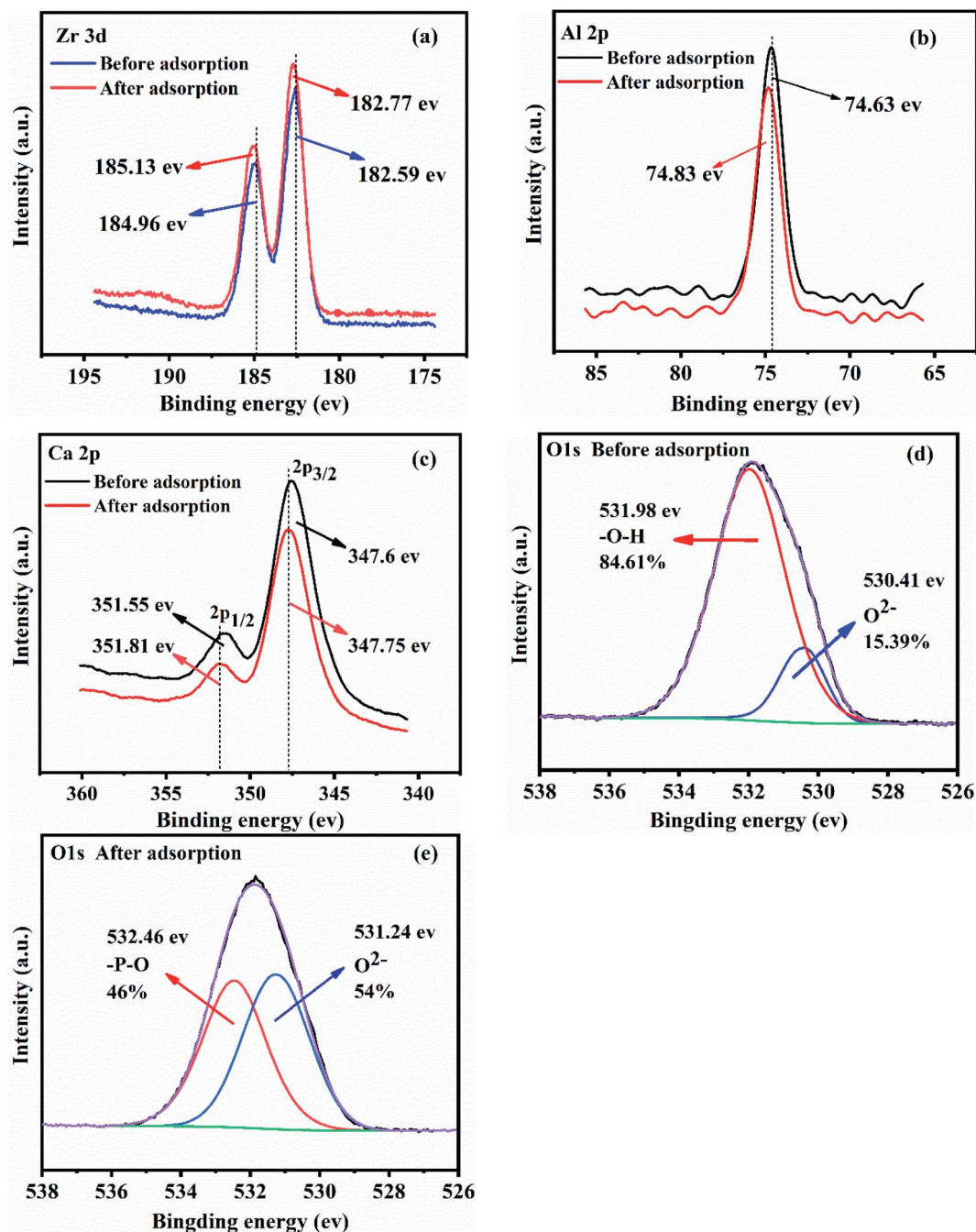

Fig. 8 XPS analysis of CGCS-Zr4 before and after phosphate adsorption: (a) Zr 3d; (b) Al 2p; (c) Ca 2p; (d) O 1s (before adsorption); (e) O 1s (after adsorption).

P–O stretching vibrations of the phosphate group, and was obviously enhanced after the reaction with phosphate, owing to its overlap with the original Si–O stretching vibration of CGCS-Zr.[39,40]

3.9.2. pH$_{pzc}$ analysis. The point of zero charge (pH$_{PZC}$) of an adsorbent is a vital parameter for determining the adsorption mechanism. As depicted in Fig. S5,† the pH$_{PZC}$ of CGCS-Zr4 was 8.41, which down shifted to 7.56 after phosphate adsorption, suggesting the formation of inner-sphere surface complexes between the phosphate anions and the CGCS-Zr4 surface.[12,41] Generally, the formation of outer-sphere complexes does not change the surface charge, whereas the formation of inner-sphere complexes usually alters pH$_{PZC}$.[12] Hence, chemical interactions and inner-sphere surface complexes played a significant role in the adsorption of phosphate ions on CGCS-Zr4. This finding is in line with the conclusion derived from ionic strength analysis.

3.9.3. XPS. To further elucidate the adsorption mechanisms of CGCS-Zr4, XPS analysis was performed to determine the variation in binding energies of some elements in CGCS-Zr4 before and after phosphate adsorption. Fig. S6(a) and (b)† show that a new P 2p peak appeared at 133.8 eV after adsorption, demonstrating the binding of phosphate to CGCS-Zr4. This result is in accordance with the EDS and FTIR results. In comparison to the basic spectrum of KH$_2$PO$_4$ (134.0 eV), the binding energy of the P 2p state is down-shifted by 0.2 eV, which is mainly attributed to the formation of chemical bonds or inner-sphere complexes between CGCS-Zr4 and phosphate.[42] The high-resolution Zr 3d spectra (Fig. 8(a)) showed the double peaks of Zr 3d$_{5/2}$ and 3d$_{3/2}$ at 182.59 and 184.96 eV, respectively, which correspond to zirconium oxide on CGCS-Zr4. After adsorption, the Zr 3d binding energies up-shifted to 182.77 and 185.13 eV, respectively, indicating that chemical interaction (complexation) occurred between Zr–O on CGCS-Zr4 and phosphate groups. The same phenomenon is observed in

Fig. 8(b); the binding energy of Al 2p (74.63 eV), corresponding to AlOOH in CGCS-Zr4, up-shifted to 74.83 eV after phosphate adsorption, indicating that Al–O–P bonds may have formed. The binding energy of Ca 2p (347.43 eV), corresponding to oxygen compounds of Ca, was also up-shifted to 347.64 eV after phosphate adsorption, as shown in Fig. 8(c). This indicates that electron transfer occurs in the adsorption process, and that Ca participates in phosphate adsorption to form Ca–O–P bonds.

These results demonstrate that, in addition to the added Zr, the Al and Ca of CGCS itself also participated in phosphate adsorption. In contrast, there was no obvious change in the Fe 2p binding energy after phosphate adsorption (Fig. S6(c)). This may be because the content of Fe in CGCS is lower than that of Al and Ca, making Fe relatively unlikely to encounter phosphate waiting to be adsorbed.

The high-resolution O 1s spectra of CGCS-Zr4 (Fig. 8(d)) fitted well to peaks of O^{2-} (530.41 eV) and –OH (531.98 eV), with O^{2-} and –OH contents of 15.39% and 84.61%, respectively. This suggests that the adsorbent contained O^{2-} and –OH.[8] After phosphate adsorption (Fig. 8(e)), it is noteworthy that the –OH peak vanished, and a new –PO peak appeared. At the same time, the proportion of O^{2-} increased by 38.61% (from 15.39% to 54%). These results could be attributed to ligand exchange between M–OH (M = Zr, Al, Ca) and phosphates (H$_2$PO$_4^-$ and HPO$_4^{2-}$), the –OH was replaced with –PO after phosphate adsorption, and finally formed Zr–O–P and Al–O–P inner-sphere complexes.

In summary, as depicted in Fig. 9, all the results discussed above demonstrate that the phosphate adsorption mechanism of CGCS-Zr4 included electrostatic attraction (discussed in detail in Section 3.2) between the protonated metal oxide surface and the phosphate anions; ligand exchange between the phosphate anions and hydroxyl groups on the metal oxide surface of CGCS-Zr4; and the generation of inner-sphere complexes, including monodentate and bidentate coordination complexes.
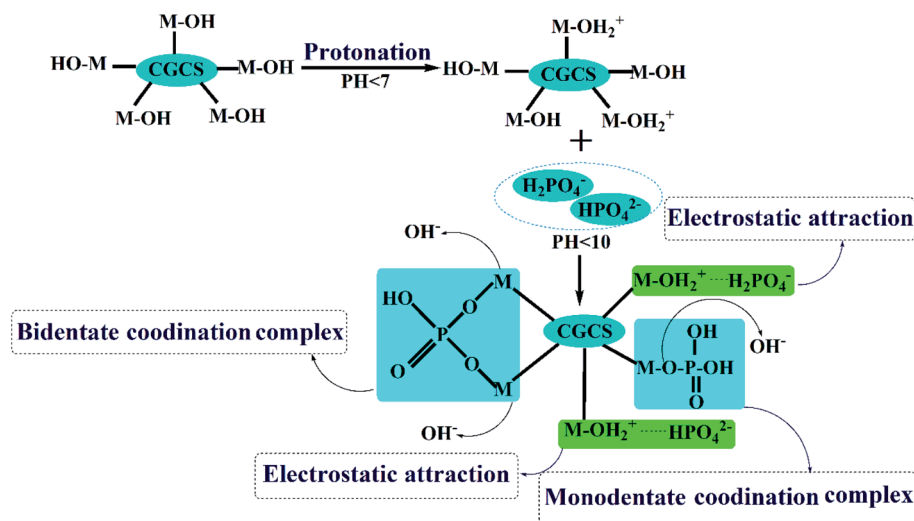

Fig. 9 Plausible mechanism of phosphate adsorption on CGCS-Zr4.

4. Conclusions

CGCS-Zr4 was prepared by a simple and energy-saving method using CGCS as an inexpensive and readily available carrier material. Compared to similar adsorbents, CGCS-Zr4 showed a higher adsorption capacity, with maximum adsorption capacities of 19.81 and 22.37 mg g^{-1} at 25 and 50 °C, respectively. The Langmuir, Elovich and intra-particle diffusion models described the experimental data well, indicating that (1) the reaction process may involve both monolayer and multilayer and occurred by chemical adsorption, and (2) the rate-determining steps were the boundary layer effect and intra-particle diffusion. The presence of competing anions has no negative effect on the adsorption of phosphate by CGCS-Zr4, and the effect of humic acid was small, indicating that CGCS-Zr4 has good adsorption selectivity for phosphate ions. The adsorption mechanism involved electrostatic attraction, ligand exchange, and the formation of inner-sphere phosphate complexes. After multiple cycles of adsorption, CGCS-Zr4 could be expected to be used as a fertiliser for vegetation growth in areas of mine restoration. Applying CGCS-Zr4 in phosphate removal can not only treat phosphate pollution in water bodies but also realise the reuse of solid waste resources, and provide a new candidate for the utilisation of CGCS.

Conflicts of interest

There are no conflicts to declare.

Acknowledgements

References

1 J. Zhou, S. Yang, J. Yu and Z. Shu, *J. Hazard. Mater.*, 2011, **192**, 1114–1121.

2 N. Karapinar, E. Hoffmann and H. H. Hahn, *Water Res.*, 2004, **38**, 3059–3066.

3 P. A. Trazzi, J. J. Leahy, M. H. B. Hayes and W. Kwapinski, *J. Environ. Chem. Eng.*, 2016, **4**, 37–46.

4 P. A. TERRY, *Environ. Eng. Sci.*, 2009, **26**, 691–696.

5 S. Sun, M. Gao, Y. Wang, Q. Qiu, J. Han, L. Qiu and Y. Feng, *Bioresour. Technol.*, 2021, **326**, 124728.

6 S. Mahdavi and D. Akhzari, *Clean Technol. Envir.*, 2016, **18**, 817–827.

7 G. Li, S. Gao, G. Zhang and X. Zhang, *Chem. Eng. J.*, 2014, **235**, 124–131.

8 W. Xiong, J. Tong, Z. Yang, G. Zeng, Y. Zhou, D. Wang, P. Song, R. Xu, C. Zhang and M. Cheng, *J. Colloid Interf. Sci.*, 2017, **493**, 17–23.

9 J. Sun, Y. Xiu, K. Huang, J. Yu, S. Alam, H. Zhu and Z. Guo, *RSC Adv.*, 2018, **8**, 22276–22285.

10 A. A. Aryee, E. Dovi, X. Shi, R. Han, Z. Li and L. Qu, *Colloids Surfaces A*, 2021, **615**, 126260.

11 Q. Xie, Y. Lin, D. Wu and H. Kong, *Fuel*, 2017, **203**, 411–418.

12 J. Huo, X. Min and Y. Wang, *Environ. Res.*, 2021, **194**, 110685.

13 S. Shan, H. Tang, Y. Zhao, W. Wang and F. Cui, *Chem. Eng. J.*, 2019, **359**, 779–789.

14 J. Xiong, L. Zang, J. Zha, Q. Mahmood and Z. He, *Sustainability*, 2019, **11**, 2453.

15 H. Gai, Y. Feng, K. Lin, K. Guo, M. Xiao, H. Song, X. Chen and H. Zhou, *Chem. Eng. J.*, 2017, **327**, 1093–1101.

16 X. Zhao, C. Zeng, Y. Mao, W. Li, Y. Peng, T. Wang, B. Eiteneer, V. Zamansky and T. Fletcher, *Energy Fuels*, 2010, **24**, 91–94.

17 D. Zhu, J. Zuo, Y. Jiang, J. Zhang, J. Zhang and C. Wei, *Sci. Total Environ.*, 2020, **707**, 136102.

18 C. Pan, Q. Liang, X. Guo, Z. Dai, H. Liu and X. Gong, *Energy Fuels*, 2016, **30**, 1487–1495.

19 S. Wang, *Chem. Ind. Eng. Prog.*, 2016, **35**, 653–664.

20 G. Dai, S. Zheng, X. Wang, Y. Bai, Y. Dong, J. Du, X. Sun and H. Tan, *J. Environ. Manage.*, 2020, **271**, 111009.

21 S. Liu, X. Chen, W. Ai and C. Wei, *J. Clean. Prod.*, 2019, **212**, 1062–1071.

22 J. Zhang, J. Zuo, W. Ai, S. Liu, D. Zhu, J. Zhang and C. Wei, *J. Hazard. Mater.*, 2020, **384**, 121347.

23 J. Zhang, J. Zuo, W. Ai, J. Zhang, D. Zhu, S. Miao and C. Wei, *Appl. Surf. Sci.*, 2021, **537**, 147938.

24 X. Huang, H. Zhao, X. Hu, F. Liu, L. Wang, X. Zhao, P. Gao and P. Ji, *J. Hazard. Mater.*, 2020, **392**, 122461.

25 Y. Abdellaoui, H. Abou Oualid, A. Hsini, B. El Ibrahimi, M. Laabd, M. El Ouardi, G. Giácoman-Vallejos and P. Gamero-Melo, *Chem. Eng. J.*, 2021, **404**, 126600.

26 Y. Su, H. Cui, Q. Li, S. Gao and J. K. Shang, *Water Res*, 2013, **47**, 5018–5026.

27 K. Zhou, B. Wu, L. Su, W. Xin and X. Chai, *Chem. Eng. J.*, 2018, **345**, 640–647.

28 A. B. M. Giasuddin, S. R. Kanel and H. Choi, *Environ. Sci. Technol.*, 2007, **41**, 2022–2027.

29 X. Min, X. Wu, P. Shao, Z. Ren, L. Ding and X. Luo, *Chem. Eng. J.*, 2019, **358**, 321–330.

30 T. Liu, S. Zheng and L. Yang, *J. Colloid Interf. Sci.*, 2019, **552**, 134–141.

31 P. Stellacci, L. Liberti, M. Notarnicola and P. L. Bishop, *Chem. Eng. J.*, 2009, **149**, 11–18.

32 K. Jung, S. Y. Lee, J. Choi and Y. J. Lee, *Chem. Eng. J.*, 2019, **369**, 529–541.

33 W. Konicki, M. Aleksandrzak, D. Moszyński and E. Mijowska, *J. Colloid Interf. Sci.*, 2017, **496**, 188–200.

34 M. Thommes, K. Kaneko, A. V. Neimark, J. P. Olivier, F. Rodriguez-Reinoso, J. Rouquerol and K. S. W. Sing, *Pure Appl. Chem.*, 2015, **87**, 1051–1069.

35 X. Luo, C. Wang, L. Wang, F. Deng, S. Luo, X. Tu and C. Au, *Chem. Eng. J.*, 2013, **220**, 98–106.

36 J. Chen, R. Yang, Z. Zhang and D. Wu, *J. Hazard. Mater.*, 2022, **421**, 126817.

37 S. Wang, L. Kong, J. Long, M. Su, Z. Diao, X. Chang, D. Chen, G. Song and K. Shih, *Chemosphere*, 2018, **195**, 666–672.

38 I. Aswin Kumar and N. Viswanathan, *Arab. J. Chem.*, 2020, **13**, 4111–4125.

39 L. S. Coulibaly, S. K. Akpo, J. Yvon and L. Coulibaly, *J. Environ. Manage.*, 2016, **183**, 1032–1040.

40 W. Shi, Y. Fu, W. Jiang, Y. Ye, J. Kang, D. Liu, Y. Ren, D. Li, C. Luo and Z. Xu, *Chem. Eng. J.*, 2019, **357**, 33–44.

41 H. Yang, X. Min, S. Xu and Y. Wang, *ACS Sustain. Chem. Eng.*, 2019, **7**, 9220–9227.

42 Y. Gu, D. Xie, Y. Ma, W. Qin, H. Zhang, G. Wang, Y. Zhang and H. Zhao, *ACS Appl. Mater. Inter.*, 2017, **9**, 32151–32160.